Available online at www.sciencedirect.com

ScienceDirect

Energy Procedia 69 (2015) 310 – 319

Energy Procedia

International Conference on Concentrating Solar Power and Chemical Energy Systems, SolarPACES 2014

Transient infrared thermography heat loss measurements on parabolic trough receivers under laboratory conditions

S.Caron[a] * , M.Röger[a], J.Pernpeintner[b]

[a]German Aerospace Center (DLR), Institute of Solar Research, Plataforma Solar de Almeria, Tabernas 04200, Spain
b German Aerospace Center (DLR); Institute of Solar Research, Cologne 51147, Germany

Abstract

This paper describes a transient infrared thermography heat loss measurement method for parabolic trough receivers and its development under laboratory conditions. The method is designed for future field measurements and represents a complementary approach to steady-state heat loss measurement methods. The receiver specific heat loss is determined by applying a thermal excitation to the absorber tube and by measuring both the absorber and glass temperature response signals with infrared pyrometers. These transient signals are processed to derive a mean absorber temperature, a mean glass temperature, an amplitude ratio and a phase shift at a mean air temperature. Temperature signals are used to identify receiver thermal properties with the help of a numerical heat transfer model coupled to a parameter identification algorithm.

Parabolic trough receivers with distinct absorber coating and annulus properties have been tested with two different transient excitation profiles, i.e. sinusoidal and ramp-and-hold signals. The identified receiver thermal properties have been compared to steady-state heat loss experiments conducted with DLR THERMOREC test bench. The observed specific heat loss deviations between steady-state and transient laboratory measurements respectively range from 2% to 4% for evacuated receivers with selective coating and from 1% to 9% for receivers with black painted absorbers.

Peer review by the scientific conference committee of SolarPACES 2014 under responsibility of PSE AG

Keywords: Parabolic Trough Receiver, Transient Infrared Thermography, Heat Loss Measurement

* Corresponding author. Tel.: +34 950 278 863; fax: + 34 950 278 863.
E-mail address: simon.caron@dlr.de

Peer review by the scientific conference committee of SolarPACES 2014 under responsibility of PSE AG
doi:10.1016/j.egypro.2015.03.035

1. Introduction

The thermal performance of a parabolic trough receiver (PTR) is defined by its overall heat loss $\dot{Q}_{th,loss}$ [W], expressed as a function of the operating absorber temperature T_{abs}. The overall radial heat loss $\dot{Q}_{th,loss}$ consists of three components and is expressed in Equation 1. The first term $\dot{Q}_{abs\text{-}gl,rad}$ accounts for the thermal radiation exchange between the outer absorber surface and the inner glass envelope surface. This term is a function of the absorber thermal emittance ε_{abs} [%]. The second term $\dot{Q}_{abs\text{-}gl,gas}$ accounts for the receiver annulus gas thermal conduction and natural convection [1].This term is a function of the annulus heat transfer coefficient h_{ann} [W/m^2.K]. The last term $\dot{Q}_{bellows}$ corresponds to the sum of radial thermal losses at each receiver bellow. The PTR overall heat loss is usually expressed as a specific heat loss per unit length $\dot{Q}'_{th,loss}$ [W/m]. The reference length $L_{rec,ref}$ is the PTR nominal length at room temperature.

$$\dot{Q}_{th,loss}\,[W] = \dot{Q}_{abs-gl,rad} + \dot{Q}_{abs-gl,gas} + \dot{Q}_{bellows}\;;\; \dot{Q}'_{th,loss}\,[W/m] = \frac{\dot{Q}_{th,loss}}{L_{rec,ref}} \quad (1)$$

PTR specific heat loss measurements have been previously performed under steady-state conditions [2] at the German Aerospace Center (DLR) [3], at the U.S. National Renewable Energy Laboratory (NREL) [4] and at the Chinese Academy of Sciences Institute of Electrical Engineering (IEECAS) [5]. The uncertainty of heat loss measurements delivered by steady-state methods is below +/- 10 W/m for laboratory test benches. Quasi-steady-state heat loss measurement methods have also been investigated under field conditions [6]. A field survey performed by NREL at the Solar Electric Generation Station (SEGS) VI power plant relied on the infrared (IR) measurement of glass envelope temperatures and a PTR numerical heat transfer model [7] for an in-situ thermal screening of several PTRs mounted in a power plant. The correlation between the specific heat loss and the stationary glass envelope temperature was shown to be highly sensitive to wind speed and ambient temperature.

An alternative heat loss measurement method based on transient IR thermography [8] has been tested at DLR. This method is designed for field PTR heat loss measurements and has been first investigated under laboratory conditions. This paper presents the experimental set-up and results of the transient IR thermography method. These are compared with steady-state heat loss measurements carried out with DLR THERMOREC test bench.

Nomenclature

A	Amplitude ratio (Units: [-])
F	Complex transfer function
G	First order system gain constant [-]
φ	Phase shift [rad]
ω	angular frequency [rad/s]
τ	First order system time constant [s]
ε_{abs}	Absorber thermal emittance [%]
ε_{shield}	Radiation shield foil thermal emittance [%]
h_{ann}	Annulus heat transfer coefficient [W/m^2.K]
$L_{rec,ref}$	Receiver nominal length at room temperature [m]
$T_{abs,o}$	Absorber tube outer surface temperature [K]
T_{air}	Air temperature inside the radiation shield [K]
T_{amb}	Ambient temperature [K]
$T_{gl,o}$	Glass envelope outer surface temperature [K]
v_{air}	Air speed inside the radiation shield [m/s]
v_{wind}	Indoor wind speed [m/s]
$\dot{Q}_{abs\text{-}gl,gas}$	Annulus gas heat transfer from the absorber tube to the glass envelope [W]
$\dot{Q}_{abs\text{-}gl,rad}$	Radiative heat transfer from the absorber tube to the glass envelope [W]
$\dot{Q}_{bellows}$	Radial heat transfer at the receiver bellows [W]
$\dot{Q}_{th,loss}$	Parabolic Trough Receiver overall heat loss [W]
$\dot{Q}'_{th,loss}$	Receiver specific heat loss per unit length [W/m]

2. Methodology

2.1. Fundamental assumptions

The transient measurement analysis workflow is summarized in Figure 1. The underlying assumption of transient heat loss measurements is that any PTR can be modeled as a Linear Time Invariant (LTI) system, i.e. a PTR can be characterized by a transfer function, which associates a glass temperature response $T_{gl,o}(t)$ to a given absorber temperature excitation $T_{abs,o}(t)$. For a stable air temperature $T_{air}(t)$, this transfer function is further assumed to correspond to a first order system [8]. The following measurands can be explicitly derived for any transient measurement: (a) amplitude ratio $A(\omega)$ [-], (b) phase shift $\varphi(\omega)$ [rad], (c) mean absorber temperature $\overline{T_{abs,o}}$ [K], (d) mean glass temperature $\overline{T_{gl,o}}$ [K], (e) mean air temperature $\overline{T_{air}}$ [K].

Temperature signals are then analyzed to determine PTR key thermal properties, i.e. the absorber thermal emittance ε_{abs} [%] and the annulus heat transfer coefficient h_{ann} [W/m^2.K]. These thermal properties are next used to simulated the PTR specific heat loss $Q'_{th,loss.}$ under standard laboratory conditions, i.e. at an ambient temperature T_{amb} of 25 °C and a wind speed v_{wind} of 0 m/s.

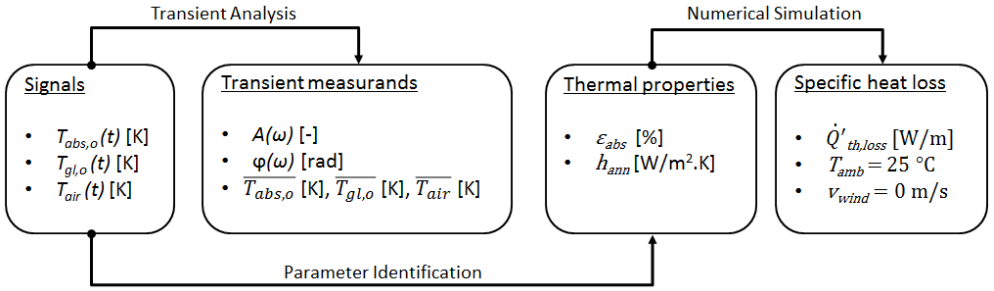

Fig. 1: Transient measurement analysis workflow.

2.2. Experimental procedure

A PTR sample is mounted according to the experimental set-up described in Section 3. The PTR is heated up until the absorber temperature reaches a pre-defined working point and the glass temperature reaches a quasi-stationary level. The emissivity factors of IR sensors are calibrated with the corresponding reference thermocouples. A transient excitation is then applied to the absorber temperature.

Two transient profiles were compared during the laboratory measurement campaign: (a) a sinusoidal signal and (b) a ramp-and-hold signal. The peak amplitude of the sinusoidal oscillation was maintained at about 10 K for the absorber temperature. The oscillation period was set to 600 seconds. 5 periods were used for the derivation of measurands. For the ramp-and-hold profile, the absorber and glass temperature were first maintained at their stationary level. The absorber temperature was then raised linearly by about 10 K within 5 minutes. Finally, the absorber temperature was maintained to a nearly constant level for at least 60 minutes, so that the glass envelope temperature reaches a new quasi-stationary level. Experimental data records are illustrated in Figure 2 for sinusoidal and a ramp-and-hold signals. Both datasets were obtained for a standard PTR at an average absorber temperature near 360°C. In both cases, the glass temperature response can be analyzed within the framework of LTI system theory to derive the amplitude ratio A and the phase shift φ measurands at the angular frequency $\omega = 2\pi/600$ [rad/s].

For sinusoidal measurements (Figure 2, top), the absorber and glass envelope temperature signals are first detrended and filtered to remove temperature drifts and outliers. These signals are then fitted to sinusoidal functions. The amplitude ratio A [-] corresponds to the ratio of the glass temperature amplitude to absorber temperature amplitude. The phase shift φ [rad] corresponds to the delay between both sinusoidal signals.

In order to derive amplitude ratio and phase shift measurands for ramp-and-hold measurements (Figure 2, bottom), the absorber and glass envelope temperature signals are first normalized, i.e. the initial offsets are subtracted. A first order system transfer function is applied to the absorber temperature signal $T_{abs,o}(t)$ to generate a virtual glass temperature response $\hat{T}_{gl,o}(t)$. The gain constant G and the time constant τ of the transfer function $F(j\omega)$ are fitted so that the difference between the measured glass temperature $T_{gl,o}(t)$ response and the virtual glass temperature response $\hat{T}_{gl,o}(t)$ is minimized according to a Least Square Method. The optimal first order transfer function $F(j\omega)$ is then exploited as outlined in Equation 2 to derive the amplitude ratio A and the phase shift φ at a given angular frequency ω. This procedure is only used to compare directly ramp-and-hold measurands with sinusoidal measurands (see Section 4.1). The identification of receiver thermal properties is described in Section 2.3.

$$F(j\omega) = \frac{G}{1 + j\omega\tau}; \quad j^2 = -1; \quad A = \frac{G}{\sqrt{1 + \omega^2\tau^2}}; \quad \varphi = -\tan^{-1}(\omega\tau) \tag{2}$$

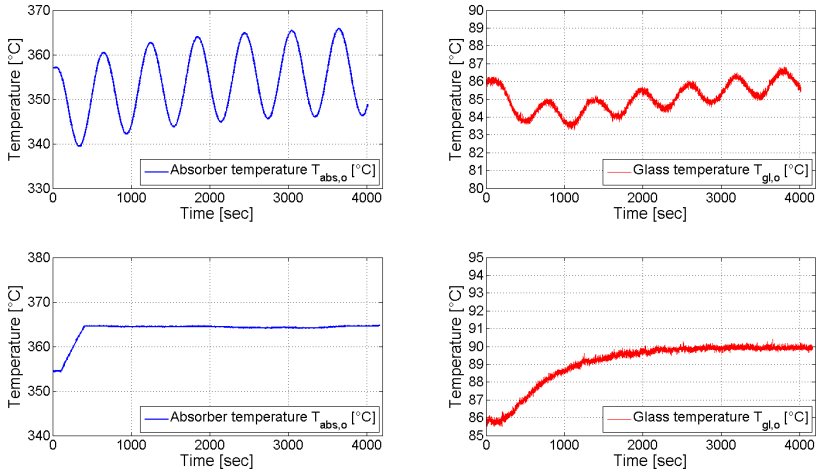

Fig. 2: Experimental data for transient measurements. (Top): Sinusoidal temperature profiles. (Bottom): Ramp-and-hold temperature profiles.

2.3. Identification of thermal properties

The next step of the transient IR heat loss measurement method is to determine PTR thermal properties from the temperature signals $\{T_{abs,o}(t); T_{gl,o}(t); T_{air}(t)\}$. For this purpose, a PTR numerical heat transfer model including a radiation shield model [8] is coupled to a hybrid optimization algorithm. The relevant model static input parameters are the absorber thermal emittance ε_{abs} [%], the annulus heat transfer coefficient h_{ann} [W/m^2.K], and the unknown air speed inside the radiation shield v_{air} [m/s]. The temperature signals $\{T_{abs,o}(t); T_{air}(t)\}$ are regarded as dynamic model inputs. The aim of the optimization algorithm is to find the optimal combination of parameters $\{\varepsilon_{abs}; h_{ann}; v_{air}\}$ that best reproduces the experimental glass temperature $T_{gl,o}(t)$. The optimization criterium δ is formulated in Equation 3. It is defined as the sum of squared deviations Δ_i, where the individual deviations Δ_i correspond to the difference between the simulated and experimental glass temperature $\left[T_{gl,o}^{meas}(t_i) - T_{gl,o}^{sim}(t_i)\right]$.

$$\delta = \left(\sum_{i=1}^{N} \frac{1}{N} \Delta_i^2\right)^{1/2} \quad ; \quad \Delta_i = \left[T_{gl,o}^{meas}(t_i) - T_{gl,o}^{sim}(t_i)\right] \tag{3}$$

The hybrid optimization algorithm combines Particle Swarm and Nelder Mead Simplex optimization algorithms. The optimization starts with a global search in a defined search space with boundary constraints, as the values of the absorber thermal emittance ε_{abs} and the annulus heat transfer coefficient h_{ann} are a priori unknown. Random model

parameter combinations are first generated for the Particle Swarm optimization algorithm. The best parameter combinations are then used as starting points for parallel searches with the Nelder Mead Simplex optimization algorithm, applying the same boundary constraints on the search space. Parameter combinations $\{\varepsilon_{abs};\ h_{ann};\ v_{air}\}_{\mathrm{opt}}$ achieving the lowest optimization criterium δ are selected and averaged to derive the best candidate solution.

2.4. Comparison with steady-state measurements

The PTR specific heat loss $\dot{Q}'_{th,loss}$ [W/m] is calculated with the parameter values $\{\varepsilon_{abs};\ h_{ann}\}$ that have been derived with the previous optimization algorithm. The heat loss calculation is performed at the average absorber temperature $\overline{T_{abs,o}}$ using the numerical heat transfer model [8] for standard laboratory conditions, at an ambient temperature T_{amb} of 25 °C and a wind speed v_{wind} of 0 m/s, without radiation shield. Simulated specific heat loss values are compared with steady-state heat loss measurements carried out with DLR THERMOREC test bench.

3. Experimental set-up

The experimental set-up built at the Plataforma Solar de Almería consists of the following items: (i) an electrical heating system, (ii) a radiation shield, (iii) infrared sensors and thermocouples, (iv) PTR test samples.

3.1. Electrical heating system

The electrical heating system is a 10 kVA transformer. The transformer secondary circuit is connected to the absorber tube with two contact terminals, which are inserted into each end. The absorber acts as an electrical resistor and is heated by Joule Effect. The voltage applied on the secondary circuit can be adjusted from 0 to 10 V with a Labview program. The voltage signal defines the transient excitation applied to the absorber temperature.

3.2. Radiation shield

A radiation shield was built for transient IR thermography measurements. This shield is shown in Figure 3. The function of this radiation shield is to reflect the IR radiation emitted by the glass envelope, so that the net radiative heat flow from the glass envelope to the ambient can be neglected. This radiation shield is also designed as a protective enclosure against environmental perturbations that may occur during field measurements, such as wind gusts or indirect solar irradiation. These perturbations would directly influence the glass temperature response and thus impact the transient measurement analysis outlined in Section 2.

The radiation shield consists of an aluminium jacket. The length of the jacket is 1360 mm, the internal diameter is 126 mm and the external diameter is 290 mm. The inner wall of the jacket is covered with an IR reflecting foil (Figure 3, right). Eight fans of diameter 60 mm are mounted on one end of the shield (Figure 3, right). These fans generate a forced convective air flow to avoid a heat build-up inside the radiation shield. The hot air leaves the shield on its other end (Figure 3, left). The outlet air velocity and air temperature are occasionally monitored with a vane anemometer. The air velocity around the PTR circumference is maintained at a low level (about 1.0 m/s) during transient measurements. The air temperature T_{air} is defined as the average between the inlet temperature (i.e. ambient temperature) and the outlet air temperature. An aperture of diameter 6 mm is drilled at the center of the radiation shield to allow IR temperature measurements of the absorber tube and glass envelope.

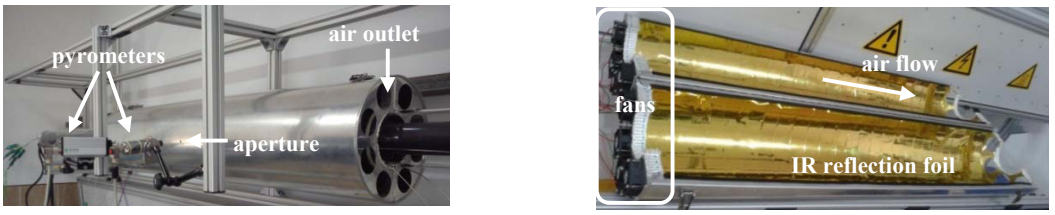

Fig. 3: Radiation shield for transient IR thermography measurements.

3.3. Temperature sensors

Twenty-four thermocouples (type K, tolerance class 1, +/- 1.5K) are positioned at various locations of the PTR, as illustrated in Figure 4. Twelve thermocouples are positioned on the absorber inner surface with metallic spring leaves. Twelve thermocouples are clamped on the glass outer surface. Thermal paste is applied to enhance their thermal contact with the glass envelope. Thermocouples are positioned symmetrically along the PTR radial and longitudinal axes. Eight thermocouples are positioned outside the radiation shield, while sixteen thermocouples are positioned within the radiation shield enclosure. Eight thermocouples positioned near the PTR mid-position are used as references for IR sensor emissivity factor calibrations. Other thermocouples are used for temperature monitoring.

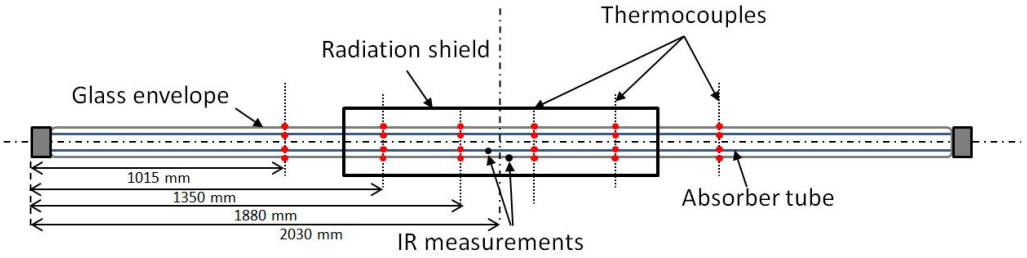

Fig. 4: Positioning of the temperature sensors in the transient IR thermography experimental set-up.

Two IR pyrometers supplied by Dias Infrared Systems GmbH are used for the temperature measurement of the absorber tube and the glass envelope. One IR pyrometer (Pyrospot DGE10N) measures the absorber temperature through the glass envelope in the wavelength band from 2.0 to 2.6 µm, as borosilicate is transparent in this domain. This wavelength band also enables to measure a broad range of operating absorber temperatures, from 100 to 600°C. Another IR pyrometer (Pyrospot DT44LH) measures the glass envelope temperature in the wavelength band from 8 to 14 µm. This wavelength domain is selected because of the expected glass temperature range, from 50 to 250°C.

3.4. PTR test samples

Three different PTR categories with similar geometrical but different coating and vacuum properties were tested during the measurement campaign, as listed in Table 1. Three samples of each category were tested under transient conditions. One PTR of each category was tested under steady-state conditions at the DLR THERMOREC test bench for cross-validation.

Table 1: Categorization of available PTR test samples for transient IR thermography measurements.

Category	Coating properties	Annulus properties	PTR Geometry
Cat. A	Selective coating (Low emittance)	Evacuated annulus (pressure $<10^{-4}$ mbar)	Absorber tube: Outer diameter: 70 mm Thickness: 2 mm Length: 4060 mm Glass envelope: Outer diameter: 125 mm Thickness: 3 mm Length: 3900 mm
Cat. B	Black paint (High emittance, ≥ 85%) Painting: Senotherm UHT 600	Evacuated annulus (pressure < 10^{-4} mbar)	
Cat. C	Black paint (High emittance, ≥ 85%) Painting: Senotherm UHT 600	Air filled annulus (pressure: ≈ 1000 mbar)	

4. Results and discussion

4.1. Analysis of transient measurands

The experimental results of the transient measurement campaign are summarized in Table 2. These results are shown for the three PTR categories outlined in Table 1, at three different operating absorber temperatures. Transient measurands are averaged for each PTR category and compared between sinusoidal (column: *Sinus*) and ramp-and-hold (column: *Ramp*) absorber temperature profiles. The deviations (column *Delta*) are defined as the difference between both sets of measurands (*Sinus* and *Ramp*) for normalized absorber temperatures.

First, it is worth observing that the absorber temperature influences all other measurands, for any PTR category. As the operating absorber temperature increases, the glass temperature and the amplitude ratio increase. The magnitude of the phase shift $|\varphi(\omega)|$ tends to decrease with increasing absorber temperatures, especially for PTRs with a black painted absorber (*Cat. B*, *Cat. C*).

The comparison of measurands between different receiver categories sets apart standard PTRs (*Cat. A)* from other PTRs (*Cat. B*, *Cat. C*). The distinction between evacuated black painted PTRs (*Cat. B*) and air filled black painted PTRs (*Cat. C*) is less obvious to detect from transient measurands. For similar operating absorber temperatures, mean glass temperatures only increase by a few Kelvins from *Cat.B* to *Cat. C*. Meanwhile, amplitude ratios increase by an order of magnitude of 0.015 and phase shifts increase by 0.02 rad.

The comparison of measurands between sinusoidal and ramp-and-hold absorber temperature profiles shows a relatively good agreement. The absolute deviations of the amplitude ratio *A* range from 0.001 [-] to 0.007 [-], with a root mean square (RMS) of 0.004 [-]. The absolute deviations of the phase shift φ range from 0.01 rad to 0.03 rad, with a RMS of 0.02 rad.

Table 2: Experimental results of the transient measurement campaign

Electrical Heating	**Measurand**	**Unit**	**PTR Cat. A (Table 1)**			**PTR Cat. B (Table 1)**			**PTR Cat. C (Table 1)**		
			Sinus	*Ramp*	*Delta*	*Sinus*	*Ramp*	*Delta*	*Sinus*	*Ramp*	*Delta*
Low (Working Point # 1)	$\overline{T_{abs,o}}$	[°C]	359.4	359.4	-	191.4	191.4	-	193.2	193.2	-
	$\overline{T_{gl,o}}$	[°C]	81.9	83.4	1.5	110.4	110.1	-0.3	114.7	115.0	0.3
	$\overline{T_{air}}$	[°C]	26.7	29.0	2.3	29.9	33.0	3.1	28.9	32.5	3.6
	$A(\omega)$	[-]	0.055	0.059	0.004	0.168	0.169	0.001	0.187	0.181	-0.006
	$\varphi(\omega)$	[rad]	-1.42	-1.43	-0.01	-1.34	-1.31	0.03	-1.32	-1.30	0.02
Mid-range (Working Point # 2)	$\overline{T_{abs,o}}$	[°C]	411.8	411.8	-	230.8	230.8	-	232.4	232.4	-
	$\overline{T_{gl,o}}$	[°C]	104.3	106.7	2.4	136.9	136.8	-0.1	141.6	142.0	0.4
	$\overline{T_{air}}$	[°C]	29.9	32.9	3.0	35.7	38.0	2.3	34.2	37.8	3.6
	$A(\omega)$	[-]	0.074	0.076	0.002	0.194	0.189	-0.005	0.211	0.210	-0.001
	$\varphi(\omega)$	[rad]	-1.40	-1.42	-0.02	-1.31	-1.29	0.02	-1.29	-1.27	0.02
High (Working Point # 3)	$\overline{T_{abs,o}}$	[°C]	457.8	457.8	-	272.2	272.2	-	271.8	271.8	-
	$\overline{T_{gl,o}}$	[°C]	128.1	130.1	2.0	166.8	166.8	0.0	169.7	170.6	0.9
	$\overline{T_{air}}$	[°C]	34.6	37.7	3.1	42.9	44.9	2.0	41.2	44.4	3.2
	$A(\omega)$	[-]	0.090	0.083	-0.007	0.221	0.219	-0.002	0.237	0.234	-0.003
	$\varphi(\omega)$	[rad]	-1.40	-1.41	-0.01	-1.29	-1.27	0.02	-1.25	-1.25	0.01

The transient IR thermography measurement method provides a qualitative distinction of receiver categories. The transient measurands *A* and φ depend on the mean absorber temperature. The comparison between sinusoidal and ramp-and-hold measurements is relatively good, although residual mismatches can be observed.

4.2. Identification of thermal properties and comparison with steady-state measurements

The temperature signals analyzed in Table 2 for ramp-and-hold excitation profiles are used for the determination of PTR thermal properties according to the method outlined in Section 2.3. In addition, specific heat loss calculations are included for each category according to the method outlined in Section 2.4. The results of this analysis are summarized in Table 3 and plotted in Figure 5. Specific heat losses are first calculated with the determined thermal properties (TRANSIENT). They are also compared with specific heat losses derived from THERMOREC steady-state measurement results and with simulated specific heat losses based on material data (Table 1). In Figure 5, specific heat loss calculations based on transient measurements are plotted with thick dashed lines, while steady-state specific heat loss measurements are plotted with full lines. Simulated specific heat loss values based on material data are also shown in thin dashed lines.

Table 3: Identification of PTR thermal properties based on transient measurements

	PTR Category (Table 1)	***Cat. A***			***Cat. B***			***Cat. C***		
	Working point	WP-A1	WP-A2	WP-A3	WP-B1	WP-B2	WP-B3	WP-C1	WP-C2	WP-C3
	$\overline{T_{abs,o}}$ [°C]	355.9	407.7	450.5	189.6	225.4	262.0	186.0	225.5	264.5
TRANSIENT	ε_{abs} [%]	11.9%	12.0%	12.6%	90.5%	92.6%	92.2%	90.2%	88.7%	91.7%
	h_{ann} [W/m^2.K]	0.064	0.013	0.032	1.57	0.498	0.207	4.56	4.40	4.58
	Optimization criterium δ	0.19	0.47	0.55	0.22	0.21	0.18	0.20	0.29	0.30
	$\dot{Q}'_{th,loss}$ [W/m] TRANSIENT (A) Standard conditions (T_{amb} = 25°C, v_{wind} = 0 m/s)	**213**	**295**	**399**	**333**	**446**	**606**	**364**	**508**	**676**
STEADY-STATE	$\dot{Q}'_{th,loss}$ [W/m] THERMOREC (B)	**208**	**307**	**407**	**331**	**466**	**639**	**334**	**484**	**666**
	Absolute deviation; (A-B) [W/m]	5	-12	-8	2	-20	-33	30	24	10
	Relative deviation; (A-B)/B [%]	+2.4%	-3.9%	-2.0%	+0.5%	-4.2%	-5.2%	+8.8%	+5.0%	+1.7%
MATERIAL DATA, SIMULATIONS	ε_{abs} [%] (material data) (FTIR Spectrophotometer)	8.8%	10.2%	11.5%	87.3%	86.9%	86.5%	87.4%	86.9%	86.5%
	h_{ann} [W/m^2.K] (specifications) (annulus pressure , Table 1)	0.013	0.013	0.012	0.013	0.013	0.013	4.49	4.58	4.63
	$\dot{Q}'_{th,loss}$ [W/m] SIMULATION (C) Standard conditions (T_{amb} = 25°C, v_{air} = 0 m/s)	**158**	**252**	**365**	**300**	**422**	**576**	**357**	**505**	**683**

The comparison of specific heat losses derived from steady-state measurements (THERMOREC) with transient specific heat loss measurements shows a very good agreement for standard PTRs (*Cat. A*) for all working points. The relative deviation ranges from -3.9% (WP-A2) to 2.0% (WP-A1).

The simulated values lie below the steady-state heat loss measurements but follow the same nonlinear trend. This deviation may be caused by a systematic bias of the FTIR spectrophotometer data for the selective coating, hence using too low thermal emittance values in the simulations. This also explains why thermal emittance values (ε_{abs}) derived from transient measurements for *Cat.A* are about 1 to 3 percentage points higher than values derived from FTIR spectrophotometer measurements.

Annulus heat transfer coefficients (h_{ann}) derived from transient measurements are slightly higher, but about the same order of magnitude than simulated values for evacuated receivers. The transient IR heat loss measurement method allows an accurate separation of heat loss mechanisms for standard receiver tubes.

The comparison of specific heat losses derived from steady-state measurements with transient specific heat loss measurements shows a similarly good agreement for *Cat.B* and *Cat.C*. The relative deviations respectively range from -5.2% (WP-B3) to +0.5% (WP-B1) for *Cat.B* and from +1.7% (WP-C3) to+8.8% (WP-C1) for *Cat.C*. In comparison to simulated values based on material data, steady-state heat loss measurements lie respectively above these values for *Cat. B* and below these values for *Cat.C*.

Thermal emittance values derived from transient measurements for *Cat.B* and *Cat.C* are slightly higher than reference ε_{abs} values derived from FTIR spectrophotometer measurements. The deviations respectively range from 3.2 (WP-B1) to 5.7 percentage points (WP-B3) for *Cat.B* and from 1.8 (WP-C2) to 5.2 percentage points (WP-C3).

Annulus heat transfer coefficients derived from transient measurements are a few orders of magnitude higher for *Cat.B* in comparison with simulated values for an annulus pressure of 10^{-4} mbar. This casts some doubt concerning the proper evacuation of *Cat.B* PTR samples, which are not standard products. Annulus heat transfer coefficients derived for *Cat.C* from transient measurements are about the same order of magnitude than expected values for an air filled annulus (1 bar). The transient IR heat loss measurement method hence allows a separation of heat loss mechanisms for non-standard receiver tubes.

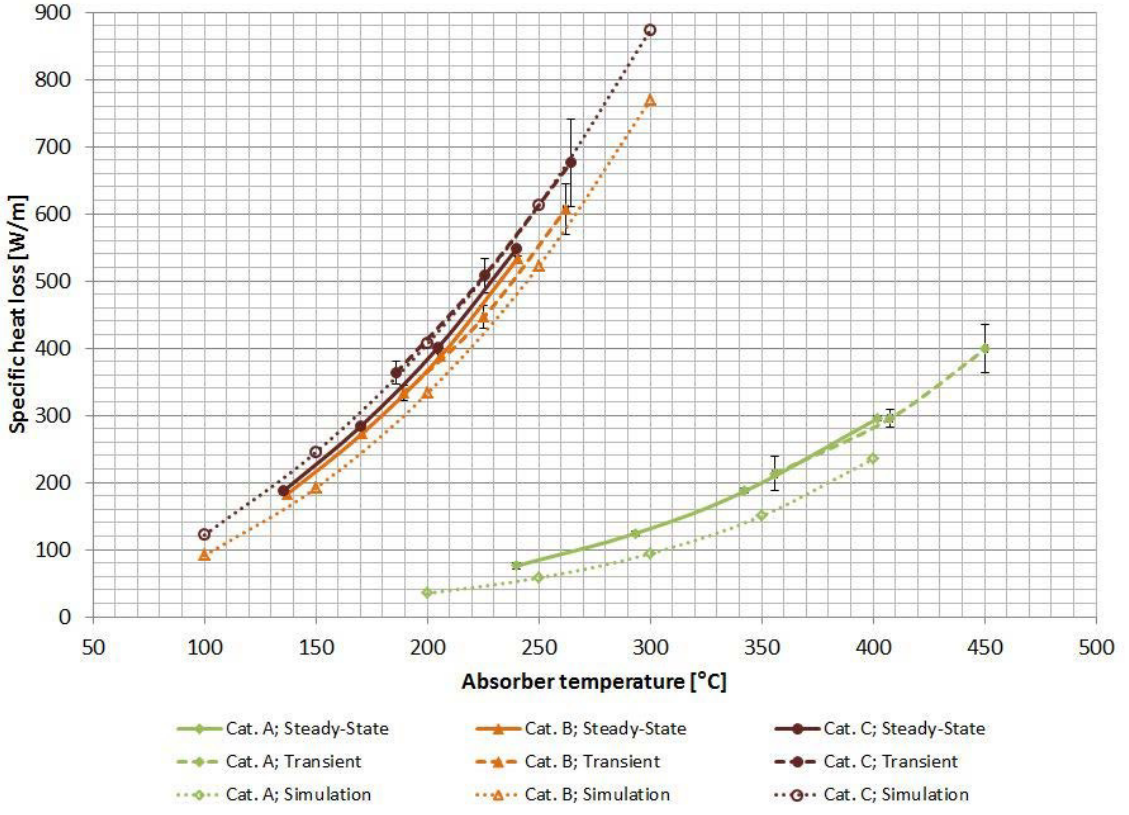

Fig. 5: Comparison between steady-state specific heat loss measurements (Steady-State), specific heat loss values derived from transient infrared thermography measurements (Transient), and simulated specific heat loss values based on material data (Simulation).

5. Conclusion and outlook

This paper presented a transient heat loss measurement method for parabolic trough receivers based on transient infrared thermography. An experimental set-up was built to test different parabolic trough receivers under transient test conditions. The experimental set-up includes a radiation shield allowing for non-destructive infrared thermography. The absorber tubes were excited with sinusoidal and ramp-and-hold temperature profiles. The absorber and glass temperature profiles were measured with infrared pyrometers. Receivers were modeled as first order linear time invariant systems. The following measurands were derived for transient experiments: mean absorber temperature, mean glass temperature, amplitude ratio, phase shift, and air temperature inside the radiation shield. A hybrid optimization algorithm coupled to a numerical PTR heat transfer model was used to determine PTR key thermal properties from the absorber and air temperature signals. These key thermal properties were used to simulate PTR specific heat losses under standard laboratory conditions.

Transient measurands could be analyzed to distinguish standard PTRs from other PTRs with high emittance black paint absorber coatings. A relatively good agreement could be observed between sinusoidal and ramp-and-hold measurements. The comparison of specific heat losses between transient and steady-state measurements showed an increasing deviation with absorber temperature for standard PTRs and a good agreement for other PTR categories. The deviation between steady-state and transient measurements respectively ranges from 2% to 4% for standard PTRs and from 1% to 9% for PTRs with high emittance black paint absorber coatings.

The identification of receiver thermal properties could yield relevant thermal emittance values and annulus heat transfer coefficients for standard PTRs. Thermal emittance values derived for PTRs with a black painted absorber (*Cat. B*, *Cat. C*) were slightly higher in comparison to FTIR spectrophotometer measurements. Annulus heat transfer coefficients were slightly overestimated for *Cat.B* PTRs and correctly estimated for *Cat.C* PTRs. The transient IR heat loss measurement method allows a relatively accurate separation of heat loss mechanisms both for standard and non-standard receiver tubes.

The transient infrared thermography method is currently tested under field conditions. First field experiments have shown the feasibility of ramp-and-hold excitation profiles for absorber tubes.

Acknowledgements

Financial support from the German Federal Ministry for Economic Affairs and Energy (PARESO Project, Contract 0325412) is gratefully acknowledged.

References

[1] Ratzel A.C, Hickox C.E., Gartling D.K., 1979, Techniques for Reducing Thermal Conduction and Natural Convection Heat Losses in Annular Receiver Geometries," ASME J. Heat Transfer, 101, pp. 108–113.
[2] Dreyer S., Eichel P., Gnaedig T., Hacker Z., Janker S., Kuckelkorn T., Silmy K., Pernpeintner J., Lüpfert E., 2010, Heat Loss Measurements on Parabolic Trough Receivers, SolarPACES 2010, Perpignan, France, September 21–24.
[3] Pernpeintner J., Anger M., Lichtenthäler N., Ant P., Happich C., Thoss J., Measurement of Parabolic Trough Receiver Thermal Loss Power and Relative Optical Efficiency under Solar Simulator Light, German Aerospace Center, DLR QUARZ Test Report (2012).
[4] Burkholder F., Kutscher C., Heat Loss Testing of Schott's 2008 PTR70 Parabolic Trough Receiver, National Renewable Energy Laboratory, Technical Report, NREL/TP-550-45633 (2009).
[5] Lei D., Li Q., Wang Z., Li J., Li J., An Experimental Study of Thermal Characterization of Parabolic Trough Receivers, Journal of Energy Conversion and Management, 69 (2013) 107-115.
[6] Price H., Forristall R., Wendelin T., Lewandowski A., Moss T., Gummo C., Field Survey of Parabolic Trough Receiver Thermal Performance, National Renewable Energy Laboratory, Conference Paper, NREL/CP-550-39459 (2006).
[7] Forristall R., Heat Transfer Analysis and Modeling of a Parabolic Trough Solar Receiver Implemented in Engineering Equation Solver, National Renewable Energy Laboratory, Technical Report, NREL TP-550-34169 (2003).
[8] Röger M., Potzel P., Pernpeintner J., Caron S., A Transient Thermography Method to Separate Heat Loss Mechanisms in Parabolic Trough Receivers, Journal of Solar Energy Engineering, 136 (2014) 011006.